J. Plasma Phys. (2018), *vol.* 84, 905840109
doi:10.1017/S0022377818000090

The Alfvénic nature of energy transfer mediation in localized, strongly nonlinear Alfvén wavepacket collisions

J. L. Verniero[1],† **and G. G. Howes**[2]

[1]Department of Mathematics, University of Iowa, Iowa City, IA 52242, USA

[2]Department of Physics and Astronomy, University of Iowa, Iowa City, IA 52242, USA

(Received 3 November 2017; revised 9 January 2018; accepted 10 January 2018)

In space and astrophysical plasmas, violent events or instabilities inject energy into turbulent motions at large scales. Nonlinear interactions among the turbulent fluctuations drive a cascade of energy to small perpendicular scales at which the energy is ultimately converted into plasma heat. Previous work with the incompressible magnetohydrodynamic (MHD) equations has shown that this turbulent energy cascade is driven by the nonlinear interaction between counterpropagating Alfvén waves – also known as Alfvén wave collisions. Direct numerical simulations of weakly collisional plasma turbulence enables deeper insight into the nature of the nonlinear interactions underlying the turbulent cascade of energy. In this paper, we directly compare four cases: both periodic and localized Alfvén wave collisions in the weakly and strongly nonlinear limits. Our results reveal that in the more realistic case of localized Alfvén wave collisions (rather than the periodic case), all nonlinearly generated fluctuations are Alfvén waves, which mediates nonlinear energy transfer to smaller perpendicular scales.

Key words: plasma nonlinear phenomena, plasma waves, space plasma physics

1. Introduction

Turbulence plays a vital role in the dynamics of space plasmas such as the solar wind, astrophysical plasma systems such as galaxy clusters and laboratory plasma environments such as magnetically confined fusion plasmas. Driven by violent events or instabilities at a large scale (such as impulsive magnetic reconnection in active regions on the Sun), turbulent energy is transferred to smaller perpendicular scales and eventually turned into plasma heat via dissipative mechanisms. Understanding the entire cascade of turbulent energy and how it converts turbulent energy into plasma heat is crucial for understanding how poorly understood astrophysical, space and laboratory plasma systems evolve. For this reason, the dynamics of the turbulent energy transfer remains a fervent research topic of plasma physics.

In contrast to the eddies that describe hydrodynamic turbulence, Alfvén waves – waves supported by magnetic tension that propagate up or down along the magnetic

† Email address for correspondence: jennifer-verniero@uiowa.edu

field – dominate the physics of turbulent motions in a magnetized plasma, a concept first proposed by early research on incompressible magnetohydrodynamic (MHD) turbulence in the 1960s (Iroshnikov 1963; Kraichnan 1965). Formulating the picture of plasma turbulence in this way, Alfvén wave collisions are known as the 'fundamental building block of plasma turbulence' (Kraichnan 1965; Howes & Nielson 2013). Hence, studying the details of the nonlinear energy transfer of Alfvén wave collisions lays important groundwork for understanding the turbulent energy cascade within a fully turbulent medium where these Alfvén wave collisions are omnipresent. Following significant work on incompressible MHD turbulence (Sridhar & Goldreich 1994; Montgomery & Matthaeus 1995; Ng & Bhattacharjee 1996; Galtier *et al.* 2000), a recent study has computed an analytical solution for the evolution of Alfvén wave collisions in the weakly nonlinear limit (Howes & Nielson 2013) which has been validated by nonlinear gyrokinetic numerical simulations (Nielson, Howes & Dorland 2013) and verified in the laboratory (Howes *et al.* 2012, 2013; Drake *et al.* 2013).

As described in detail in Howes & Nielson (2013), the general picture of nonlinear energy transfer in the weakly nonlinear case is as follows. Alfvén wave modes are of the form $\hat{\boldsymbol{k}} = (k_x/k_{\perp 0}, k_y/k_{\perp 0}, k_z/k_{\parallel 0})$, where $k_{\perp 0}$ and $k_{\parallel 0}$ are the perpendicular and parallel wavenumbers relative to the equilibrium magnetic field direction of the initial two Alfvén waves in the MHD limit, $k_\perp \rho_i \ll 1$. First, the perpendicularly polarized primary Alfvén wave modes $\hat{\boldsymbol{k}}_1^- = (1, 0, 1)$ and $\hat{\boldsymbol{k}}_1^+ = (0, 1, -1)$ interact nonlinearly to give $\hat{\boldsymbol{k}}_1^- + \hat{\boldsymbol{k}}_1^+ = \hat{\boldsymbol{k}}_2^{(0)} = (1, 1, 0)$. Under the periodic conditions adopted to facilitate an analytical solution, the secondary mode is a purely magnetic fluctuation, physically representing a shear in the magnetic field which oscillates at a rate of $2\omega_A$, where $\omega_A \equiv k_{\parallel 0} v_A$ is the frequency of the two primary Alfvén waves. This inherently nonlinear mode has no parallel variation ($k_\parallel = 0$), therefore it is not an Alfvén mode since it does not satisfy the Alfvén wave dispersion relation, $\omega = k_\parallel v_A$. In other words, this $\hat{\boldsymbol{k}}_2^{(0)}$ mode does not propagate as an Alfvén wave, which would have a parallel phase velocity $\omega/k_\parallel = v_A$ and a parallel group velocity $\partial\omega/\partial k_\parallel = v_A$. Furthermore, the amplitude of this secondary mode rises and falls in an oscillatory fashion at a frequency of $2\omega_A$, never gaining energy secularly. This secondary mode is essentially a nonlinearly generated beat mode (Drake *et al.* 2016). Next, each primary mode $\hat{\boldsymbol{k}}_1^\pm$ interacts with this secondary mode $\hat{\boldsymbol{k}}_2^{(0)}$ to transfer energy secularly to two tertiary modes, $\hat{\boldsymbol{k}}_1^\pm + \hat{\boldsymbol{k}}_1^{(0)} = \hat{\boldsymbol{k}}_3^\pm$, where $\hat{\boldsymbol{k}}_3^- = (2, 1, 1)$ and $\hat{\boldsymbol{k}}_3^+ = (1, 2, -1)$. These tertiary modes $\hat{\boldsymbol{k}}_3^\pm$ have the same value of $k_\parallel$ as the corresponding primary modes $\hat{\boldsymbol{k}}_1^\pm$. The amplitude of these tertiary modes $\hat{\boldsymbol{k}}_3^\pm$ grows secularly in time, with energy transfer from the primary modes $\hat{\boldsymbol{k}}_1^\pm$ mediated by the strictly oscillatory secondary mode $\hat{\boldsymbol{k}}_0^{(0)}$. The analytical calculation (Howes & Nielson 2013) therefore identifies the key role of the nonlinearly generated secondary mode with $k_\parallel = 0$ in the nonlinear transfer of energy from larger to smaller perpendicular scales relative to the background magnetic field. The purpose of the present study is to illuminate the nature of this secondary mode in the more realistic case of collisions between initially separated Alfvén wavepackets.

Strongly nonlinear MHD plasma turbulence simulations have led to another important discovery about plasma turbulence, that intermittent current sheets develop (Matthaeus & Montgomery 1980; Meneguzzi, Frisch & Pouquet 1981) and turbulent energy dissipation is mostly concentrated within these sheets (Uritsky *et al.* 2010; Osman *et al.* 2011; Zhdankin *et al.* 2013). Therefore, evidence for the connection between the development of current sheets and the dissipation of turbulent energy into

https://doi.org/10.1017/S0022377818000090 Published online by Cambridge University Press

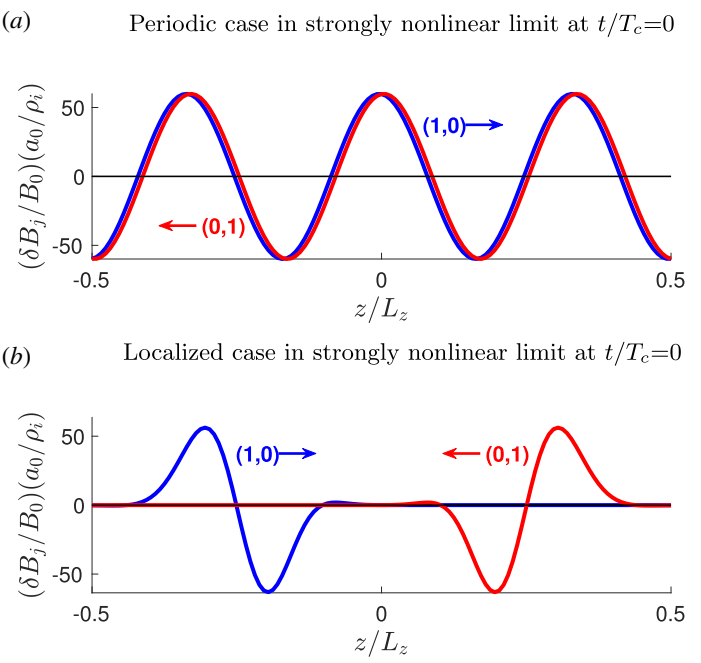

FIGURE 1. Set-up for perpendicularly polarized Alfvén waves in the localized and periodic cases. Note that the blue curve corresponds to the $(k_x, k_y) = (1, 0)$ mode and the red curve corresponds to the $(k_x, k_y) = (0, 1)$ mode. Note that the blue and red fluctuations are polarized perpendicularly to each other, with δB_x (red) and δB_y (blue).

plasma heat has been sought after observationally (Borovsky & Denton 2011; Osman *et al.* 2011, 2012; Perri *et al.* 2012; Wang *et al.* 2013; Wu *et al.* 2013; Osman *et al.* 2014) and numerically (Wan *et al.* 2012; Karimabadi *et al.* 2013; TenBarge & Howes 2013; Wu *et al.* 2013; Zhdankin *et al.* 2013). Recent work has shown that in the strong turbulence limit, Alfvén wave collisions generate current sheets (Howes 2016), an important breakthrough connecting the self-consistent development of intermittent current sheets and the nonlinear mechanism responsible for transferring turbulent energy to smaller scales. Subsequent work using the new field–particle correlation technique (Klein & Howes 2016; Howes 2017; Howes, Klein & Li 2017; Klein & TenBarge 2017) has shown that the particle energization in these current sheets involves collisionless energy transfer via the Landau resonance (Howes, McCubbin & Klein 2018).

The previous work on Alfvén wave collisions (Howes & Nielson 2013; Nielson *et al.* 2013) explored the nonlinear interactions between two perpendicularly polarized, counterpropagating plane Alfvén waves under periodic boundary conditions. These two plane Alfvén waves were initially overlapping before they began to interact nonlinearly, an unrealistic, idealized set-up that enabled an asymptotic analytical solution to be obtained in the weakly nonlinear limit. A depiction of the initial conditions in this case is shown in figure 1(*a*), where the variation of the magnetic field, $\boldsymbol{B}$, along the direction z (parallel to the equilibrium magnetic field) for each of the two initial, perpendicularly polarized Alfvén waves is plotted. The upward propagating Alfvén wave has a δB_y polarization with a perpendicular Fourier mode $(1, 0)$ (blue) and the downward propagating Alfvén wave has a δB_x polarization

https://doi.org/10.1017/S0022377818000090 Published online by Cambridge University Press

with a perpendicular Fourier mode (0, 1) (red). Note these initial plane Alfvén wave modes fill the simulation domain and are periodic in both the perpendicular plane as well as the parallel direction. We refer to this Alfvén wave initialization as the periodic case. Note that the periodic boundary conditions are not what makes this scenario unrealistic, but rather the fact that the two waves started on top of each other and consequently did not arrive in those positions while undergoing a self-consistent nonlinear interaction.

An important question is whether the key properties of the nonlinear evolution of Alfvén wave collisions found in this idealized periodic case persists for the more realistic case of the interaction between two initially separated Alfvén wavepackets. To answer this question, we perform nonlinear kinetic simulations of the interaction between two localized Alfvén wavepackets that do not initially overlap, as shown in figure 1(*b*). Here, the upward propagating Alfvén wave has a δB_y polarization but the wavepacket is localized along the field parallel direction around $z = -L_z/4$, where L_z denotes the length of the simulation domain. Note that this Alfvén wavepacket remains periodic in the perpendicular plane, with its variation given by the Fourier mode (1, 0) (blue). The downward propagating Alfvén wave has a δB_x polarization, is localized in z around $z = L_z/4$, and corresponds to a perpendicular Fourier mode (0, 1) (red). Although the simulation domain itself is periodic in the z direction, such that a wave propagating in the $+z$ direction will exit the domain at $z = L_z/2$ and re-enter the domain at $z = -L_z/2$, the localization of the wavepackets along z means that these two wavepackets will not interact nonlinearly until they come together and overlap along z, a more realistic situation. We refer to this initially separated Alfvén wavepacket initialization as the localized case.

Our previous study of strongly nonlinear, localized Alfvén wave collisions (Verniero, Howes & Klein 2018) found that indeed nonlinear interactions between initially separated wavepackets facilitate the cascade of energy to smaller perpendicular scales relative to the background magnetic field and self-consistently give rise to current sheets, just as found in the periodic case. But that study employed asymmetric initial Alfvén wavepackets (see figure 1 of Verniero *et al.* 2018), where one of the wavepackets had a significant $k_\parallel = 0$ component initially relative to the background magnetic field. Since it is the secondary mode with $k_\parallel = 0$ that plays the key role in mediating the secular transfer of energy to smaller perpendicular scales in the periodic case, it is important to ensure that the non-zero $k_\parallel = 0$ component of the wavepacket in Verniero *et al.* (2018) does not affect the results in a fundamental way. To address this issue, we pursue here a detailed comparison of periodic Alfvén wave and localized Alfvén wavepacket collisions, where the initial wavepackets are symmetric and neither wavepacket has a significant $k_\parallel = 0$ component. This study will enable us to determine the nature of the nonlinearly generated modes that mediate the cascade of energy to smaller perpendicular scales relative to the background magnetic field in the localized case and to ensure that the non-zero $k_\parallel = 0$ component in the Verniero *et al.* (2018) study did not qualitatively alter the resulting cascade by artificially initializing a mode that dominates the nonlinear energy transfer.

We aim to answer two primary questions: (i) what is the nature of the nonlinearly generated secondary mode that mediates the cascade of energy in localized Alfvén wave collisions?; and (ii) how does the localization of the interacting Alfvén waves into separated wavepackets affect the qualitative and quantitative evolution of the perpendicular cascade of energy and the development of current sheets?

In § 2, we describe the set-up of the simulation for each of the four cases being compared. The nonlinear energy evolution of each case is presented in § 3.1. Our

https://doi.org/10.1017/S0022377818000090 Published online by Cambridge University Press

results in § 3.2 show that the secondary (1, 1) mode is an Alfvén wave mode. The strongly and weakly nonlinear limits are compared in § 3.3. Current sheet development is confirmed in § 3.4. Conclusions are discussed in § 4.

2. Simulation

The nonlinear interaction between two counterpropagating localized Alfvén wavepackets or periodic Alfvén waves is simulated using the astrophysical gryokinetics code `AstroGK` (Numata *et al.* 2010). `AstroGK` evolves the perturbed gyroaveraged distribution function $h_s(x, y, z, \lambda, \varepsilon)$ for each species s, the scalar potential φ, the parallel vector potential $A_\parallel$ and the parallel magnetic field perturbation $\delta B_\parallel$ according to the gyrokinetic equation and the gyroaveraged Maxwell equations (Frieman & Chen 1982; Howes *et al.* 2006). Velocity space coordinates are $\lambda = v_\perp^2/v^2$ and $\varepsilon = v^2/2$. The domain is a periodic box of size $L_\perp^2 \times L_z$, elongated along the straight, uniform mean magnetic field $\boldsymbol{B}_0 = B_0\hat{\boldsymbol{z}}$, where all quantities may be rescaled to any parallel dimension satisfying $L_z/L_\perp \gg 1$. Uniform Maxwellian equilibria for ions (protons) and electrons are chosen, with a realistic mass ratio $m_i/m_e = 1836$. Spatial dimensions (x, y) perpendicular to the mean field are treated pseudospectrally; an upwind finite-difference scheme is used in the parallel direction, z. Collisions employ a fully conservative, linearized collision operator with energy diffusion and pitch-angle scattering (Abel *et al.* 2008; Barnes *et al.* 2009).

To reveal details of the turbulent transfer of energy through the interaction of Alfvén waves, we directly compare four simulations runs:

(i) Localized Alfvén wavepacket collisions in the strongly nonlinear limit, `LS`.
(ii) Periodic Alfvén wave collisions in the strongly nonlinear limit, `PS`.
(iii) Localized Alfvén wavepacket collisions in the weakly nonlinear limit, `LW`.
(iv) Periodic Alfvén wave collisions in the weakly nonlinear limit, `PW`.

For all cases, the plasma parameters are ion plasma beta $\beta_i = 1$ and ion-to-electron temperature ratio $T_i/T_e = 1$. We choose a perpendicular simulation domain size $L_\perp = 40\pi\rho_i$ with simulation resolution $(n_x, n_y, n_z, n_\lambda, n_\varepsilon, n_s) = (32, 32, 128, 32, 16, 2)$ such that our initial Alfvén waves fall into the MHD limit, $k_\perp\rho_i \ll 1$. The fully resolved perpendicular range in this dealiased pseudospectral method covers $0.05 \leqslant k_\perp\rho_i \leqslant 0.5$. Here the ion thermal Larmor radius is $\rho_i = v_{ti}/\Omega_i$, the ion thermal velocity is $v_{ti}^2 = 2T_i/m_i$, the ion cyclotron frequency is $\Omega_i = q_iB_0/(m_ic)$ and the temperature is given in energy units. The parallel length of the simulation domain is L_z, extending over the range $[-L_z/2, L_z/2]$. Note that the simulation domain is triply periodic, so when a wavepacket exits the domain at $z = \pm L_z/2$, it re-enters at the opposite end at $z = \mp L_z/2$, enabling the two wavepackets to undergo successive collisions with each other. The linearized Landau collision operator (Abel *et al.* 2008; Barnes *et al.* 2009) is employed with collisional coefficients $\nu_i = \nu_e = 10^{-3}k_\parallel v_A$, yielding weakly collisional dynamics with $\nu_s/\omega \ll 1$.

The initial Alfvén wavepackets have perpendicular wave vectors $\boldsymbol{k}_\perp^-\rho_i = (k_x\rho_i, k_y\rho_i) = (0.05, 0)$ for the upward (z^-) wavepacket and $\boldsymbol{k}_\perp^+\rho_i = (k_x\rho_i, k_y\rho_i) = (0, 0.05)$ for the downward (z^+) wavepacket, so both waves have the same initial perpendicular wavenumber $k_\perp^\pm\rho_i = 0.05$, but are polarized perpendicular to each other. For brevity, we will refer to modes normalized to the domain scale perpendicular wave vector $k_{\perp 0} \equiv 2\pi/L_\perp$, giving $\boldsymbol{k}_\perp^-/k_{\perp 0} = (k_x/k_{\perp 0}, k_y/k_{\perp 0}) = (1, 0)$.

Figure 1 illustrates the initial conditions for both the (*a*) periodic and (*b*) localized cases. In (*a*), we plot the waveforms for the periodic cases, which are exactly the

https://doi.org/10.1017/S0022377818000090 Published online by Cambridge University Press

same as the localized case but without the application of the windowing function in z, so that the localized and periodic cases are directly comparable. Here we plot the waveforms along the parallel direction z at $t = 0$ of the perpendicular Fourier mode $(k_x/k_{\perp 0}, k_y/k_{\perp 0}) = (1, 0)$ of δB_y (blue) and of the perpendicular Fourier mode $(0, 1)$ of δB_x (red) for the localized Alfvén wavepacket case in (*b*). The localization along the $+z$ direction is specified using the procedure outlined in appendix A of Verniero *et al.* (2018) with the parameters $k_z a_0 = 3$, $\delta = 0$, $z_0 = -\pi/2a_0 = -L_\parallel/4$, $\Delta_z = 1.2a_0$ and an exponent $p = 2$. For the wave which propagates in the $-z$ direction, the parameters are $k_z a_0 = -3$, $\delta = 0$, $z_0 = \pi/2a_0 = L_\parallel/4$, $\Delta_z = 1.2a_0$ and an exponent $p = 2$. Figure 1 shows the amplitudes for the strongly nonlinear (*a*) periodic and (*b*) localized cases; the weakly nonlinear cases have the same initial waveforms but smaller amplitudes.

The amplitude of the initial wavepackets is parameterized by the nonlinearity parameter (Goldreich & Sridhar 1995), defined by taking the ratio of the magnitudes of the linear to the nonlinear terms in the incompressible MHD equations (Howes & Nielson 2013; Nielson *et al.* 2013). In terms of Elsasser variables, defined by $z^\pm = \boldsymbol{u} \pm \delta \boldsymbol{B}/\sqrt{4\pi(n_{0i}m_i + n_{0e}m_e)}$, the nonlinearity parameter is defined by $\chi^\pm \equiv |z^\mp \cdot \nabla z^\pm|/|\boldsymbol{v}_A \cdot \nabla z^\pm|$, where $\chi^\pm$ characterizes the strength of the nonlinear distortion of the $z^\pm$ Alfvén wave by the counterpropagating $z^\mp$ Alfvén wave. For the particular initial Alfvén wavepackets shown in figure 1, the nonlinearity parameter simplifies to $\chi^\pm = 2k_\perp \delta B_\perp^\mp/(k_\parallel B_0)$. With the $z^\pm$ wavepackets having parallel wavenumbers of approximately $k_\parallel a_0 = \mp 3$, where $a_0 = L_z/2\pi$, the amplitude of the wavepackets in the strongly nonlinear case $(\delta B_\perp^\pm/B_0)(a_0/\rho_i) \simeq 60$ gives $\chi^\pm = 2$ and the amplitude of the wavepackets in the weakly nonlinear case $(\delta B_\perp^\pm/B_0)(a_0/\rho_i) \simeq 4$ gives $\chi^\pm = 0.13$. Critically balanced, strong turbulence corresponds to a nonlinearity parameter of $\chi \sim 1$ (Goldreich & Sridhar 1995), and weak turbulence corresponds to $\chi \ll 1$, so these simulations fall into the desired limits of strong and weak nonlinearity, respectively.

3. Results

The nonlinear evolution of the localized and periodic strong and weak Alfvén wave collisions during the first few collisions is concisely illustrated by a plot of the evolution of the energy in particular perpendicular Fourier modes in figure 2. A meaningful quantitative comparison between the localized cases and the periodic cases is made possible by selecting comparable energies for each Fourier mode and a suitable definition of the Alfvén wave collision time scale in each case.

First, because the waveform in the z direction differs between the localized and periodic cases, we choose to integrate the energy of each perpendicular Fourier mode $(k_x/k_{\perp 0}, k_y/k_{\perp 0})$ along the z direction to facilitate comparison.

Second, we choose to normalize our time scales to the appropriate time scale of a single complete Alfvén wave collision in both the localized and periodic cases. In the localized case, the wavepackets collide twice during the time it takes for an Alfvén wave to propagate the parallel length of the domain, defined by $T_{L_z} \equiv L_z/v_A$. By comparison, each wavelength in the periodic case passes through three wavelengths of the counterpropagating waves during one wave-crossing period T_{L_z}. Therefore, we define the collision time as $T_c^{(l)} = T_{L_z}/2$ for the localized Alfvén wavepacket collision case and $T_c^{(p)} = T_{L_z}/3$ for the periodic Alfvén wave collision case. To further illustrate the evolution in the localized case, note that the first collision begins when the counterpropagating wavepackets begin to overlap in z at $t/T_c^{(l)} = 1/6$ and ends at $t/T_c^{(l)} = 5/6$. Subsequently, the second collision begins at $t/T_c^{(l)} = 7/6$ and ends at $t/T_c^{(l)} = 11/6$.

https://doi.org/10.1017/S0022377818000090 Published online by Cambridge University Press

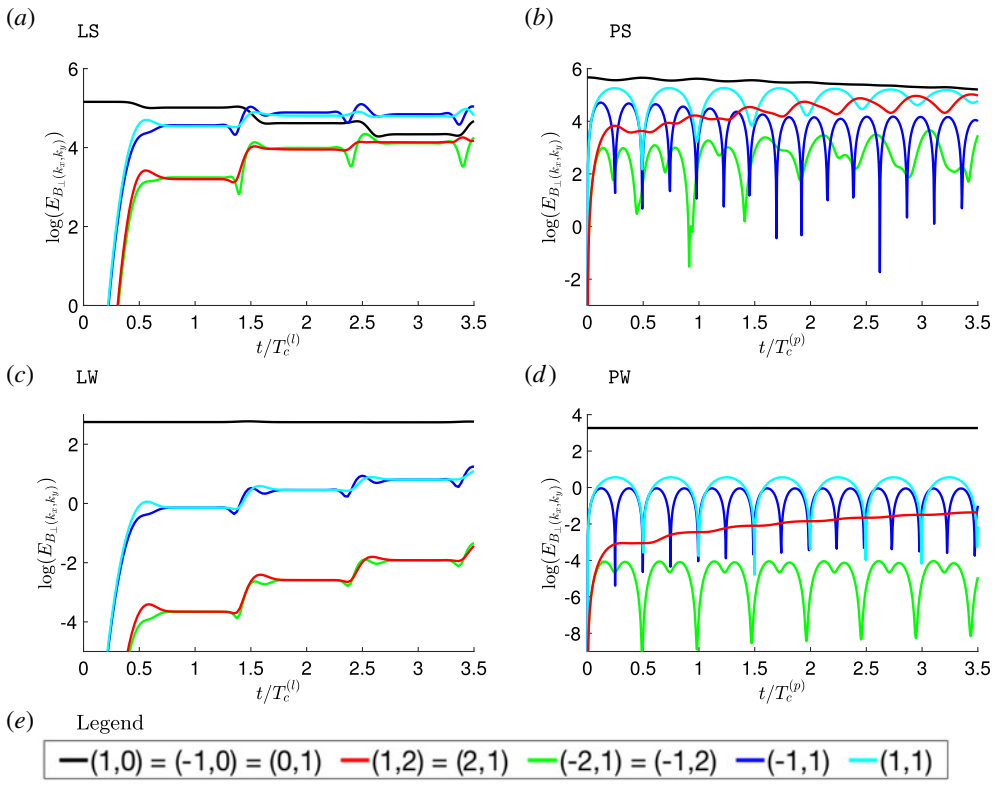

FIGURE 2. Energy evolution of each case for key (k_x, k_y) modes after 3 collisions, for the (*a*) localized, strongly nonlinear case LS, (*b*) periodic, strongly nonlinear case PS, (*c*) localized, weakly nonlinear case LW and (*d*) periodic, weakly nonlinear case PW.

3.1. *Evolution of energy of secondary* (1, 1) *mode*

The temporal evolution of energy of select (k_x, k_y) modes for the first three collisions is shown in figure 2 while figure 3 shows the full time evolution of the simulations. To illustrate differences between the periodic and localized cases, we first focus on the weakly nonlinear limit. From (*d*), in the periodic case, the evolution agrees with the analytical solution from Howes & Nielson (2013), as described qualitatively above in § 1. Notice that the secondary (1, 1) mode, which mediates the secular transfer of energy to the tertiary (1, 2) and (2, 1) modes, does not experience a net gain in energy. This (1, 1) mode corresponds to the inherently nonlinear fluctuation that does not propagate, as described in the introduction. In contrast, the secondary (1, 1) mode of the localized case in (*c*) clearly does gain energy, which is the most consequential difference among all the curves. This means that in the localized case, this secondary mode gains energy like all other nonlinearly generated modes. One other major distinction between LW and PW is that in LW, energy is only transferred during periods when the wavepackets overlap in z, giving the energy evolution curve a stair-step appearance. In contrast, PW has persistent energy transfer since the wavepackets never separate.

Note that convergence studies have been done to verify that the results with this $(n_x, n_y) = (32, 32)$ resolution are accurately resolved by the grid in AstroGK. We initially started this experiment using a resolution of $(n_x, n_y) = (10, 10)$ and replicated

https://doi.org/10.1017/S0022377818000090 Published online by Cambridge University Press

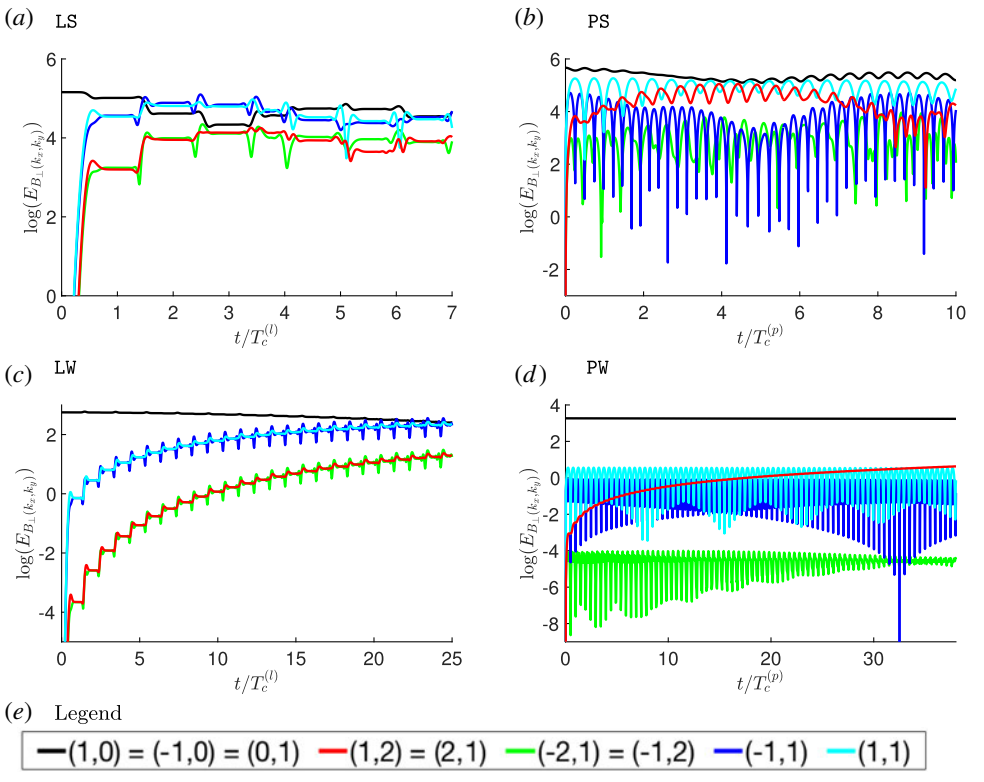

FIGURE 3. Full energy evolution of each case for key (k_x, k_y) modes, for the (*a*) localized, strongly nonlinear case LS, (*b*) periodic, strongly nonlinear case PS, (*c*) localized, weakly nonlinear case LW and (*d*) periodic, weakly nonlinear case PW.

the same results using $(n_x, n_y) = (16, 16)$. For the $(n_x, n_y) = (32, 32)$ case, we followed the evolution of energy until it deviated from the (16, 16) resolution case and ceased the simulation at that point. The results presented in figure 3 follow the evolution of energy up until the time step of this deviation point for each of the localized and periodic cases in the weakly and strongly nonlinear limit. At the end of the time evolution shown in figure 3, approximately 13 % of the initial magnetic energy has been transferred nonlinearly to higher $k_\perp$ modes (not shown in the figure) for case LS and about 17 % of the initial magnetic energy for case PS.

3.2. *Identification of nonlinearly generated modes as Alfvén waves*

In the periodic case, as reviewed in the introduction, the secondary (1, 1) mode mediates the secular transfer of energy from the primary Alfvén waves to the tertiary Alfvén waves, and this mode is an inherently nonlinear fluctuation that satisfies neither the linear eigenfunction relation nor the linear dispersion relation for an Alfvén wave. For the more realistic case of localized Alfvén wavepacket collisions, we aim to determine here the nature of the secondary (1, 1) mode. Specifically, we ask whether this secondary (1, 1) mode is an Alfvén wave. A linear Alfvén wave must satisfy two conditions (Howes & Nielson 2013): (i) it satisfies the linear eigenfunction relation for an Alfvén wave, $\boldsymbol{u}_\perp/v_A = \pm\delta\boldsymbol{B}_\perp/B_0$; and (ii) it has a frequency given by the linear Alfvén wave dispersion relation, $\omega = \pm k_\parallel v_A$. The strongly nonlinear localized

https://doi.org/10.1017/S0022377818000090 Published online by Cambridge University Press

case LS is the most relevant to the case of heliospheric plasma turbulence, so we focus strictly on this case below.

3.2.1. *Alfvén wave eigenfunction relation*

To confirm that the fluctuations that are nonlinearly generated by the LS Alfvén wave collisions have the character of linear Alfvén waves, we first verify that the electric field, $\boldsymbol{E}$, and magnetic field fluctuations are related by the following linear eigenfunction relation (Howes & Nielson 2013)

$$\frac{\boldsymbol{B}_\perp}{B_0} = \pm \frac{c\boldsymbol{E}_\perp}{v_A B_0} \times \hat{\boldsymbol{z}}, \tag{3.1}$$

where the positive sign corresponds to an Alfvén wave travelling down the magnetic field in the $-z$ direction, and the negative sign corresponds to an Alfvén wave travelling up the magnetic field in the $+z$ direction.

Separating the two components perpendicular to the equilibrium magnetic field $\boldsymbol{B}_0 = B_0\hat{\boldsymbol{z}}$ given by (3.1), we note that Alfvén waves travelling up the magnetic field in the $+z$ direction will satisfy the relations

$$\frac{B_x}{B_0} = -\frac{cE_y}{v_A B_0}, \quad \frac{B_y}{B_0} = +\frac{cE_x}{v_A B_0} \tag{3.2a,b}$$

and that Alfvén waves travelling down the magnetic field in the $-z$ direction will satisfy the relations

$$\frac{B_x}{B_0} = +\frac{cE_y}{v_A B_0}, \quad \frac{B_y}{B_0} = -\frac{cE_x}{v_A B_0}. \tag{3.3a,b}$$

For notational simplicity, we use a hat to denote these dimensionless magnetic and electric field components, $\hat{B}_j \equiv B_j/B_0$ and $\hat{E}_j \equiv cE_j/(v_A B_0)$. Note that the propagation direction of the Alfvén wave is easily determined by computing the Poynting flux, $\boldsymbol{S} = (c/4\pi)\boldsymbol{E} \times \boldsymbol{B}$.

In figure 4, we present normalized $\hat{\boldsymbol{E}}$ and $\hat{\boldsymbol{B}}$ field components of the primary, secondary and tertiary modes in the (*a–c*, *d–f* and *g–i*, respectively) at times $t/T_c^{(l)} = 0,\ 1,\ 2$ (in the first, second and third columns, respectively). In the first column of figure 4 at $t/T_c^{(l)} = 0$, we have only (*a*) the primary Alfvén wavepackets. The upward propagating Alfvén wave has a perpendicular variation given by the $(1, 0)$ Fourier mode and has a magnetic field polarization in the y direction. This wavepacket satisfies the normalized eigenfunction for an upward propagating Alfvén wave, $\hat{B}_y = \hat{E}_x$ (red/black). The downward propagating Alfvén wave has a perpendicular variation given by the (0, 1) Fourier mode and has a magnetic field polarization in the x direction. This wavepacket satisfies the normalized eigenfunction for a downward propagating Alfvén wave, $\hat{B}_x = \hat{E}_y$ (blue/green). In addition, at $t/T_c^{(l)} = 0$, (*d*) the secondary (1, 1) Fourier mode and (*g*) the tertiary (1, 2) Fourier mode are zero.

In figure 4(*b*,*e*,*h*), we show the primary, secondary, and tertiary modes after the first collision at $t/T_c^{(l)} = 1$. In figure 4(*b*), the primary Alfvén waves have passed through each other completely and still satisfy the same linear Alfvén wave eigenfunction relations as before the first collision in (*a*). Shown in (*e*), energy has been transferred to the secondary (1, 1) Fourier mode, in two separate localized wavepackets, each with magnetic field components in both the x and y direction. At $z < 0$, the downward

https://doi.org/10.1017/S0022377818000090 Published online by Cambridge University Press

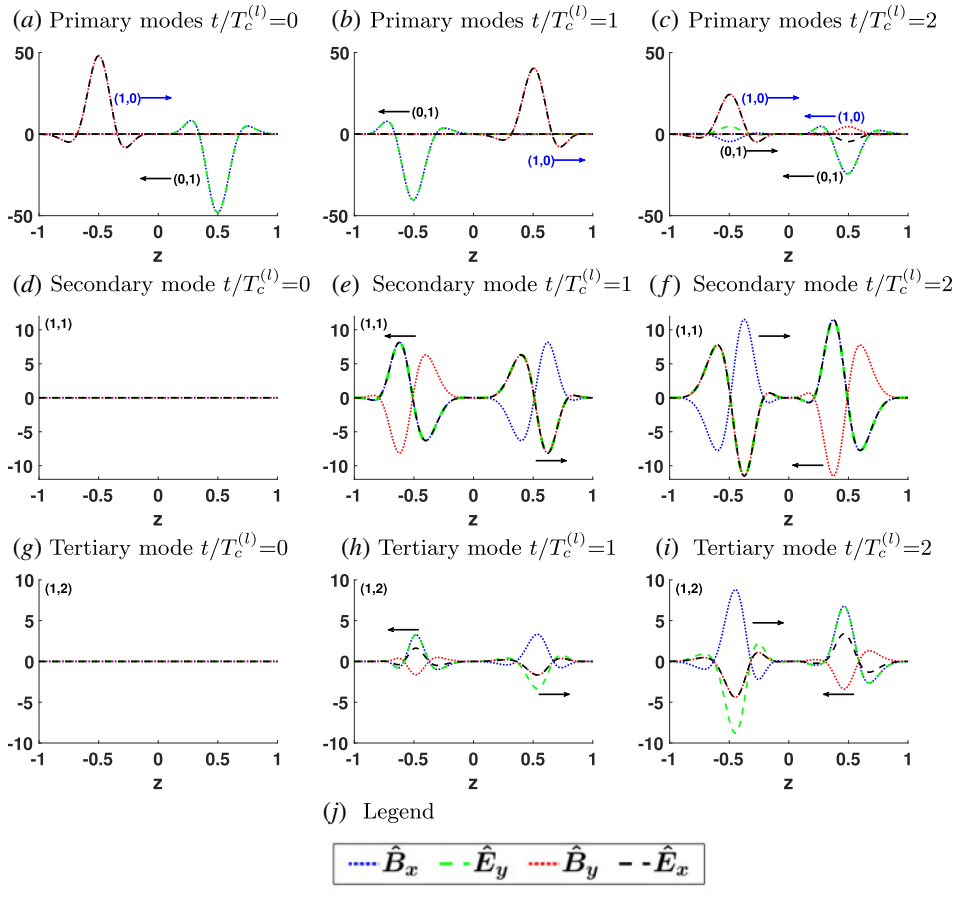

FIGURE 4. Snapshots in time of $\hat{B}_x$ (blue, dotted), $\hat{E}_y$ (green, dashed), $\hat{B}_y$ (red, dotted) and $\hat{E}_x$ (black, dashed) of select (k_x, k_y) Fourier modes in the LS case. The first, second and third rows correspond to the primary, secondary and tertiary modes respectively. All times are normalized to the localized Alfvén collision time, $T_c^{(l)}$. The black arrows indicate the direction of motion of the two colliding wavepackets.

propagating wavepacket satisfies the eigenfunction relations $\hat{B}_y = -\hat{E}_x$ (red/black) and $\hat{B}_x = \hat{E}_y$ (blue/green), as expected for a downward travelling Alfvén wave. At $z > 0$, the upward propagating wavepacket satisfies the eigenfunction relations $\hat{B}_y = \hat{E}_x$ (red/black) and $\hat{B}_x = -\hat{E}_y$ (blue/green), as expected for an upward travelling Alfvén wave. This confirms that this secondary (1, 1) mode satisfies the linear Alfvén wave eigenfunction. Shown in (*h*), the tertiary (1, 2) Fourier mode also involves two separate localized wavepackets with magnetic field components in both the x and y direction. A close inspection of the curves confirms that this tertiary (1, 2) mode also satisfies the linear Alfvén wave eigenfunction.

In figure 4(*c*,*f*,*i*), we show the primary, secondary and tertiary modes after the second collision at $t/T_c^{(l)} = 2$. In (*c*), the upward and downward moving Fourier wavepackets have developed a component of polarization perpendicular to their original polarizations. For instance, the upward wavepacket, which initially (at $t/T_c^{(l)} = 0$) consisted of only a (1, 0) Fourier mode with magnetic field polarized in the

https://doi.org/10.1017/S0022377818000090 Published online by Cambridge University Press

y direction (red), now has a smaller (0, 1) Fourier mode contribution moving in the $+z$ direction that has a magnetic field polarized in the x direction (blue). Similarly, the downward moving wavepacket, originally solely involving a (0, 1) Fourier mode polarized in the x direction (blue), now also includes a smaller contribution from a (0, 1) mode polarized in the y direction (red). These newly generated contributions to the upward and downward moving wavepackets gained energy through nonlinear energy transfer from other modes during the second collision. The secondary and tertiary modes at $t/T_c^{(l)} = 2$ in panels (*f*) and (*i*) also show an increase in amplitude relative to $t/T_c^{(l)} = 1$, showing that nonlinear interactions in the second collision have further transferred energy to those modes from the primary Alfvén wavepackets.

Another way to visualize the upward and downward propagating Alfvén waves is to compute the Elssaser fields, $\boldsymbol{z}^{\pm}$. Specifically, we write the components of the normalized Elssaser variables for the upward (z^-) and downward (z^+) Alfvén waves as

$$\hat{z}_x^{\pm} \equiv \frac{z_x^{\pm}}{v_A} = \frac{cE_y}{v_A B_0} \pm \frac{\delta B_x}{B_0} \tag{3.4}$$

and

$$\hat{z}_y^{\pm} \equiv \frac{z_y^{\pm}}{v_A} = -\frac{cE_x}{v_A B_0} \pm \frac{\delta B_y}{B_0}. \tag{3.5}$$

In figure 5, we plot the downward travelling Elsasser components z_x^+ (black) and z_y^+ (red) and the upward travelling Elsasser components z_x^- (green) and z_y^- (blue) for the same primary (*a–c*), secondary (*b–f*) and tertiary (*g–i*) modes shown in figure 4. Note that in each of the two separate, counterpropagating wavepackets, the downward moving components (red/black) are always together in the same wavepacket localized in z, and likewise the upward moving components (blue/green) are always together, confirming the fact that these wavepackets remain localized in their extent along the equilibrium magnetic field.

The main message from figures 4 and 5 is that, in the localized, strongly nonlinear Alfvén wavepacket collision (LS) case, all of the nonlinearly generated components of the Alfvén wavepackets satisfy the linear Alfvén wave eigenfunction condition given by (3.1). This includes the secondary (1, 1) Fourier mode, which does not satisfy this eigenfunction condition in the periodic case (Howes & Nielson 2013; Nielson *et al.* 2013). Note that this characteristic of the difference between the periodic Alfvén wave and localized Alfvén wavepacket collisions is true in both the weakly and strongly nonlinear limits (not shown).

3.2.2. *Alfvén wave dispersion relation*

In the MHD limit $k_\perp \rho_i \ll 1$, the Alfvén wave satisfies the linear dispersion relation $\omega = |k_\parallel| v_A$, where we adopt the convention that $\omega \geqslant 0$, so the sign of $k_\parallel$ indicates the direction of propagation of a plane Alfvén wave along the equilibrium magnetic field, $\boldsymbol{B}_0 = B_0 \hat{\boldsymbol{z}}$. This simple dispersion relation indicates that Alfvén waves are non-dispersive. The parallel phase velocity is given by $v_{p_\parallel} = \omega/k_\parallel = \pm v_A$ and indicates that wave crests of constant phase propagate up or down the equilibrium magnetic field at the Alfvén speed, v_A. The parallel group velocity is given by $v_{g_\parallel} = \partial\omega/\partial k_\parallel = \pm v_A$, meaning that the envelope of an Alfvén wavepacket will propagate up or down the equilibrium magnetic field at the Alfvén speed, v_A.

https://doi.org/10.1017/S0022377818000090 Published online by Cambridge University Press

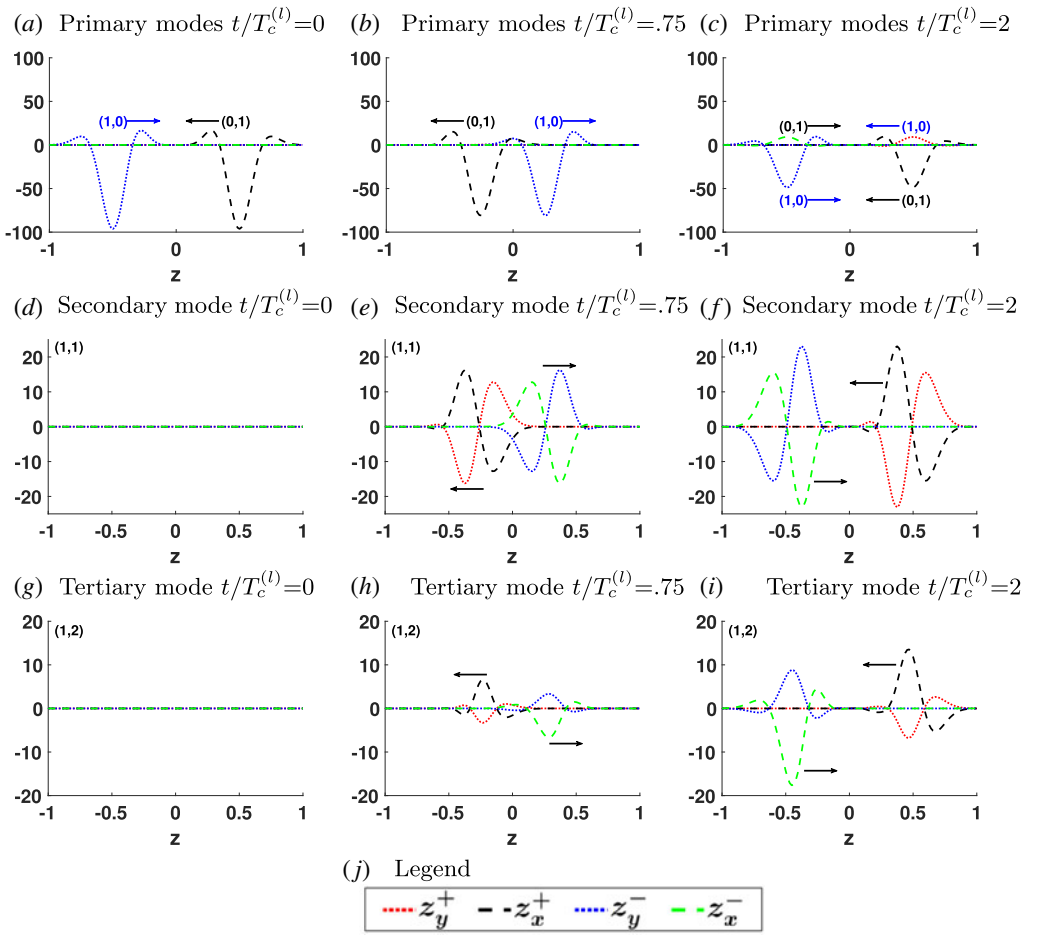

FIGURE 5. Snapshots in time of perpendicular Elssaser field components z_y^+ (red, dotted), z_x^- (green, dashed), z_y^- (blue, dotted) and z_x^+ (black, dashed) of key (k_x, k_y) modes in the LS case. The first, second and third rows correspond to the primary, secondary and tertiary modes respectively. All times are normalized to the localized Alfvén collision time, $T_c^{(l)}$. The black arrows indicate the direction of motion of the two colliding wavepackets.

A brute-force determination of whether any nonlinearly generated mode satisfies the linear Alfvén wave dispersion relation requires a decomposition of the fluctuation into plane-wave modes to enable a comparison between the parallel wavenumber $k_\parallel$ of each constituent plane-wave mode and its linear frequency ω. Such a task is complicated for the case of collisions between localized Alfvén wavepackets, which necessarily contain a broad spectrum of parallel wavenumbers to accomplish localization in z. But the non-dispersive nature of Alfvén waves makes an alternative approach possible: if the nonlinearly generated modes propagate along the equilibrium field direction together with the original Alfvén wavepackets at the Alfvén speed, then collectively they describe a localized wavepacket propagating non-dispersively. In figure 6, we overplot the perpendicular magnetic field perturbation $\delta B_\perp$ of the secondary (1, 1) Fourier mode with that of the primary (0, 1) and (1, 0) Fourier modes at times $t/T_c^{(l)} = 1, 2, 3$, showing that the nonlinearly generated (1, 1) mode does

https://doi.org/10.1017/S0022377818000090 Published online by Cambridge University Press

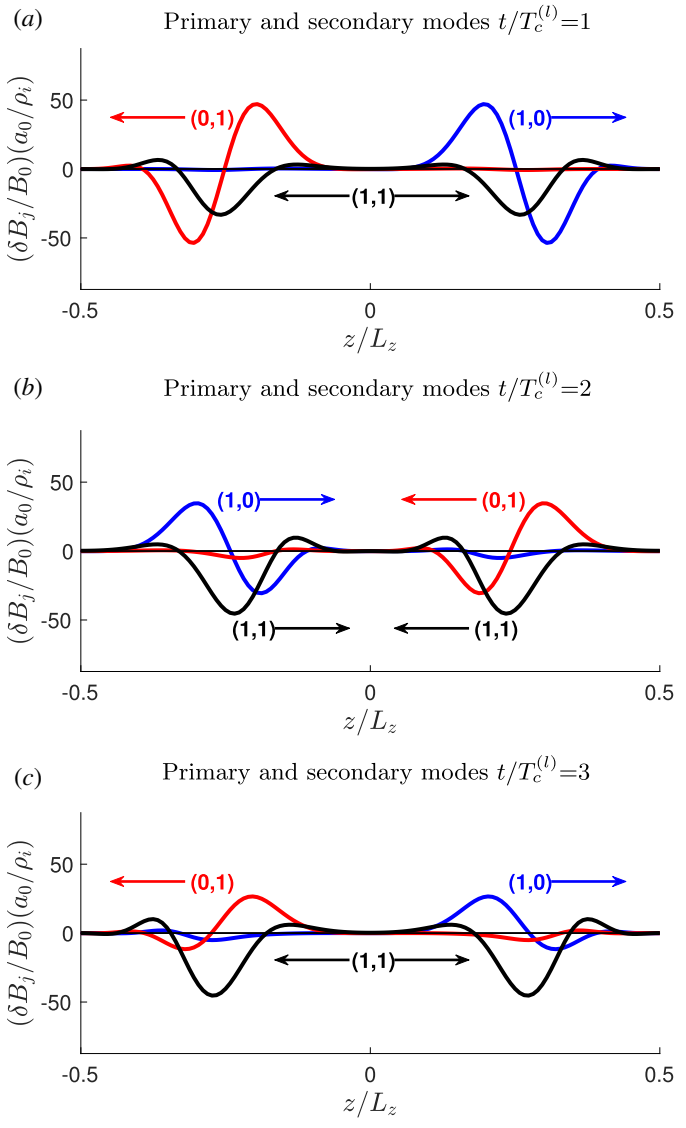

FIGURE 6. Snapshots in time of $\delta B_\perp$ versus z of primary modes (1, 0) and (0, 1) overlapping the secondary mode (1, 1) in the LS case. All times are normalized to the localized Alfvén collision time, $T_c^{(l)}$.

indeed propagate up or down along z with the primary modes at the Alfvén speed. Furthermore, as predicted from the analytical solution for Alfvén wave collisions (Howes & Nielson 2013; Howes *et al.* 2013), the (1, 1) mode is phase shifted by $\pi/2$ relative to the primary mode from which it gained energy. For example, in figure 6(*a*), the downward (0, 1) mode (red) passes through zero at the same position in z at which the downward propagating secondary (1, 1) mode (black) reaches a peak. The crucial point of figure 6 is that, in the localized Alfvén wavepacket collision, the nonlinearly generated, secondary (1, 1) Fourier mode satisfies the linear Alfvén wave dispersion relation, propagating along the equilibrium magnetic field non-dispersively.

https://doi.org/10.1017/S0022377818000090 Published online by Cambridge University Press

It is worthwhile noting that the gyrokinetic simulations performed here indeed captures the physics of the finite-ion-Larmor-radius corrections that cause the Alfvén wave solution to become dispersive at $k_\perp \rho_i \to 1$, transitioning to the dispersive kinetic Alfvén wave. Therefore, there is a very slight spreading of the wavepackets after nonlinear interactions have transferred energy into modes with $k_\perp \rho_i \gtrsim 1$. This behaviour is noticeable in figure 7 of our companion paper (Verniero *et al.* 2018) and is discussed in more detail in section 3.4 of that paper.

In summary, the results presented in figures 4 and 5 show that, in the more realistic strong, localized Alfvén wavepacket collision case, the secondary (1, 1) mode satisfies the linear Alfvén wave eigenfunction condition. The results presented in figure 6 show that this mode also satisfies the linear Alfvén wave dispersion relation. Therefore, we conclude that this secondary (1, 1) Fourier mode, which plays a key role in the nonlinear transfer of energy to smaller perpendicular scales, is simply an Alfvén wave. Note that one may interpret this (1, 1) mode of the Alfvén wave as a shear that propagates along the magnetic field at the Alfvén speed (Howes & Bourouaine 2017). This finding leads to a simplification of the picture of the nonlinear cascade of energy in plasma turbulence relative to the idealized (but analytically soluble) periodic case. In the periodic case, the nonlinear energy transfer to smaller scales is mediated by an inherently nonlinear (1, 1) Fourier mode. In the more realistic localized case, the energy mode that mediates the energy transfer is simply an Alfvén wave itself, both gaining energy from the nonlinear interaction and mediating further energy transfer to smaller scales.

3.3. *Strong versus weak turbulence*

Although the primary aim of this study is to understand how the physics of Alfvén wave collisions changes in the more realistic case of localized Alfvén wavepacket collisions, it is also worthwhile to explore the differences between the weak and strong cases in both the periodic and localized cases.

In figures 2 and 3, comparing the (*d*) weakly and (*b*) strongly nonlinear periodic cases, the most obvious difference is that the energy of the primary Alfvén waves is significantly diminished in the strongly nonlinear case, whereas in the weakly nonlinear case, the loss of energy by the primary Alfvén waves is negligible, even over the long time scale shown in figure 3(*d*), as expected. What is not necessarily expected is that the evolution between the strongly and weakly nonlinear periodic cases is qualitatively similar, with the secondary (1, 1) mode and the tertiary (1, 2) and (2, 1) Alfvén waves as the dominant recipients of the energy nonlinearly transferred from the primary Alfvén waves. The physics governing the nonlinear cascade of energy to smaller scales appears to be similar in the weakly and strongly nonlinear limits, suggesting that physical intuition from the weakly nonlinear limit provides a useful framework for the interpretation of the strongly nonlinear dynamics. Such an approach, in fact, underlies the recent discovery that strong Alfvén wave collisions naturally develop current sheets (Howes 2016). A final qualitative feature of the long-term evolution in the PS case, shown in figure 3(*b*), is that the primary Alfvén waves lose energy up to $t/T_c^{(p)} \sim 5$, and then their amplitudes begin to rise again. This curious behaviour arises from the dispersive nature of kinetic Alfvén waves in the limit $k_\perp \rho_i \to 1$. The nonlinearly generated tertiary Alfvén waves in the gyrokinetic system have a slight dispersive increase in their frequency due to finite-Larmor-radius averaging, and over time begin to shift out of phase with the primary modes, eventually transferring some of their energy back to the primary waves (Nielson 2012).

https://doi.org/10.1017/S0022377818000090 Published online by Cambridge University Press

Comparing the (*c*) weakly and (*a*) strongly nonlinear localized cases in figures 2 and 3, we observe the same qualitative similarity between the weakly and strongly nonlinear dynamics, with a more significant fraction of energy lost by the primary Alfvén wavepackets in the strongly nonlinear case, again as expected. In contrast to the periodic cases, in both weakly and strongly nonlinear localized cases, all nonlinearly generated modes gain energy secularly over time. Because all of these smaller perpendicular scale modes are gaining energy, there is a substantially greater loss of energy from the primary Alfvén wavepackets in the `LW` case relative to the loss from the primary Alfvén waves in the `PW` case, clearly shown by comparing figure 3(*c*,*d*). The strongly nonlinear `LS` and `PS` cases in figure 3(*a*,*b*) show a similar relation, where the energy loss from the localized case is much more significant than in the periodic case. Therefore, it appears that localized Alfvén wavepacket collisions are much more effective in mediating the nonlinear cascade to smaller perpendicular scales. This is a key result because the localized, strongly nonlinear `LS` case, the primary focus of this paper, is the most physically relevant case for application to particular space and astrophysical environments, such as the solar wind and solar corona.

3.4. *Current sheet development*

The final aim of this paper is to determine whether current sheets naturally develop in the localized case of a strongly nonlinear collision between two symmetric Alfvén wavepackets, where neither initially has a substantial $k_\parallel = 0$ component. Figure 7 shows plots of the normalized parallel current density $j_z/j_0 = (j_z/n_{0i}q_i v_{ti})(a_0/\rho_0)$ in the (x, y) plane perpendicular to the equilibrium magnetic field.

Figure 7(*a*,*c*,*e*) follows the evolution of the upward propagating z^- Alfvén wavepacket, while (*b*,*d*,*f*) shows the downward propagating z^+ Alfvén wavepacket. Note that the waves collide at the midpoint of the simulation box $z = 0$ and periodically at the end points $z = \pm L_z/2$. We plot the perpendicular cross-section of the parallel current density j_z of each wavepacket at $z = \pm L_z/4$ when the wavepackets are not overlapping at $t/T_c^{(l)} = 0$ in (*a*,*b*), after the first collision at $t/T_c^{(l)} = 1$ in (*c*,*d*), and after the second collision at $t/T_c^{(l)} = 2$ in (*e*,*f*). In (*c*,*d*), we see that the nonlinear distortion of the original current pattern persists after the first collision, leading to a narrowing and intensification of the current sheet. After the second collision in (*e*,*f*), the current density has further thinned and intensified into a sheet-like morphology. Note that the amplitude of the colour scale increases with later snapshots, making it clear that the current sheets are becoming increasingly intense and narrow over time. Therefore, the result first shown in Verniero *et al.* (2018), that strong localized Alfvén wavepacket collisions naturally lead to the development of current sheets, is not dependent on the non-zero $k_\parallel = 0$ component of one of the colliding Alfvén wavepackets in that study. We may therefore conclude that the development of current sheets in strong, localized Alfvén wavepacket collisions is a robust result that is not dependent on any particular forms of the initial wavepackets, further extending the impact of the initial discovery that strong Alfvén wave collisions self-consistently generate current sheets (Howes 2016), providing a first-principles explanation for the ubiquitous observations of current sheets in turbulent space and astrophysical plasmas.

4. Conclusion

The results presented in this paper settles the issue of the nature of the nonlinearly generated secondary mode – the mode that mediates the nonlinear transfer of energy

https://doi.org/10.1017/S0022377818000090 Published online by Cambridge University Press

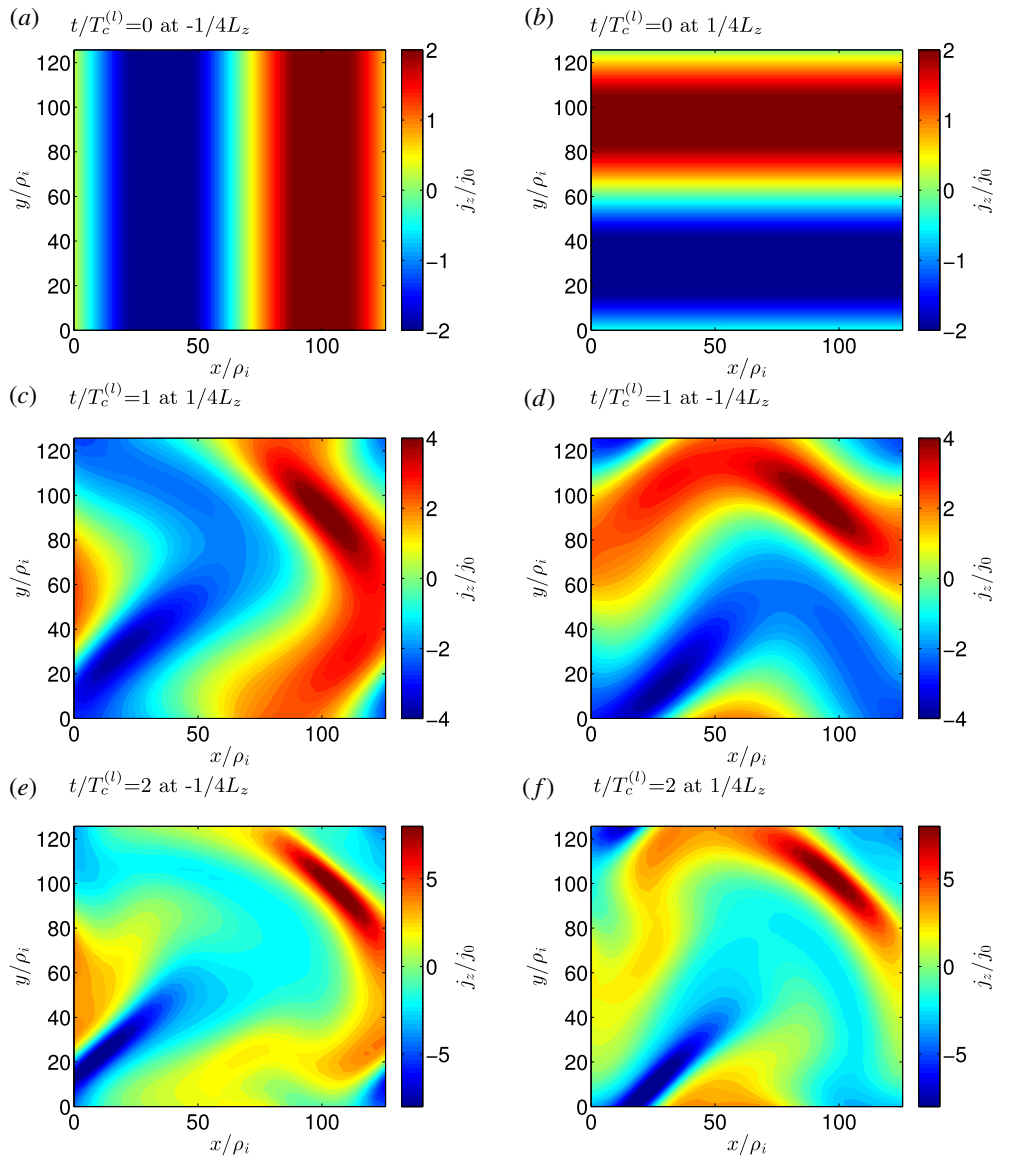

FIGURE 7. Current sheet formation before and after each collision of case LS.

in Alfvén wave collisions – in a more realistic setting than the idealized periodic case that was used in previous work to enable an analytical solution to be computed. Addressing the first question in the introduction, we conclude that these secondary modes are indeed Alfvén modes in the case of localized Alfvén wavepacket collisions. This fact was confirmed by showing (i) the eigenfunction condition, that there is the correct relationship between the $\boldsymbol{E}$ and $\boldsymbol{B}$ fields described by (3.1) and shown in figures 4 and 5 and (ii) the correct frequency condition, that the (1, 1) mode travels at the Alfvén speed in accordance with the rest of the energy modes as shown in figure 6.

https://doi.org/10.1017/S0022377818000090 Published online by Cambridge University Press

Observing figures 2 and 3, we found that in the periodic cases, only the tertiary (1, 2) and (2, 1) modes experience a secular gain of energy after successive collisions, while in the localized cases, the secondary (1, 1) mode gains energy in addition to the tertiary modes. This means that in the case of localized wave collisions in both the strongly and weakly nonlinear limit, energy transfer to smaller perpendicular scales is more efficient than in the periodic case. We also saw, by comparison between the weakly and strongly nonlinear cases, that the primary modes in the strongly nonlinear limit lose significantly more energy than the weakly nonlinear cases. This saturation is the most discernible quantitative difference between strong and weak turbulence, while most other key features remain qualitatively similar such as overall evolution of the energy of different perpendicular Fourier modes in time. We conclude that the strong, localized LS case is the most effective way to transfer energy to smaller perpendicular scales. This particular case of localized, strong turbulence, the focal point of this paper, is the most applicable case to space and astrophysical plasmas. Hence, this case is crucial for understanding the various turbulent energy cascades within our universe such as black hole accretion disks, the solar wind and planetary magnetospheres.

From figure 7, we have also demonstrated that for the strong, localized LS case, self-consistent current sheets are generated after successive collisions and persist in between collisions, consistent with previous findings on strong turbulence simulations for both the periodic (Howes 2016) and initially asymmetric localized cases (Verniero *et al.* 2018). This particular finding shows that Alfvén wavepacket collisions in the strongly nonlinear limit are a robust mechanism for current sheet development, regardless of initial waveform. In turbulent space and astrophysical plasmas, current sheets are observed ubiquitously and have been proposed to play a key role in the conversion of turbulent energy into plasma heat. The quest to understand how a plasma becomes heated is currently an active topic of research in the plasma physics community. For example, the Parker Solar Probe, due to be launched in July 2018, will investigate how the solar corona becomes heated to unprecedented temperatures, a topic that has been debated for decades. The result presented in this paper – that localized, strongly nonlinear Alfvén wave collisions naturally produce current sheets – means that the observations of current sheets in many space and astrophysical plasma systems can be explained from first principles.

We conclude that in the most physically applicable case of localized, strongly nonlinear interactions, the fundamental properties of plasma turbulence still persist: energy cascades nonlinearly to smaller perpendicular scales and intermittent current sheets are self-consistently generated, answering the second question posed in the introduction. In Verniero *et al.* (2018), we analysed the case of localized, strongly nonlinear Alfvén wavepacket collisions with asymmetric initial waveforms. The symmetric conditions presented in this paper demonstrate clearly that the effect of a non-zero $k_{\parallel}$ component does not alter the main characteristics of the Alfvén wave collisions that govern plasma turbulence.

Our findings of the Alfvénic nature of the key (1, 1) mode in the localized, strongly nonlinear case is a satisfying simplification of the picture of the nonlinear energy transfer to small scales in plasma turbulence. It is important to emphasize the fact that an Alfvén wave collision is the fundamental unit of interaction in plasma turbulence (Kraichnan 1965; Howes & Nielson 2013), and a turbulent plasma would contain many such nonlinear interactions among upward and downward propagating Alfvén wavepackets. Such an *ab initio* approach to this subject allows for a clearer picture to be painted and consequently enables deeper insight about the dynamics. The results presented in this paper highlight the central role played by Alfvén waves

https://doi.org/10.1017/S0022377818000090 Published online by Cambridge University Press

in the nonlinear cascade of energy. The generation of the secondary mode mediates the transfer of energy from the primary to tertiary modes. The secondary mode is essentially a shear in the magnetic field that propagates along the magnetic field as an Alfvén wave, shearing the perpendicular waveform of counterpropagating Alfvén wavepackets and thereby nonlinearly transferring their energy to smaller perpendicular scales (Howes & Bourouaine 2017). In contrast to the idealized periodic case, this secondary (1, 1) mode gains energy secularly along with all of the other nonlinearly generated modes. The striking difference between the periodic case with two initially overlapping plane Alfvén waves and the localized Alfvén wavepacket case raises the question of whether the non-Alfvénic 'beat' modes that arise in the periodic case will alter the statistics of the turbulence. For decaying turbulence simulations, in which the initialized Alfvénic fluctuations are already overlapping as in our periodic case, this is an issue that merits further investigation. A follow-up study could investigate the role of the Alfvénic propagating shear, discussed in this paper, on magnetic field line wander, enabling a more atomistic description of the tangling of magnetic field lines within the framework of Alfvén wave collisions. Our analysis of the more realistic case of localized Alfvén wave collisions brings us closer to understanding the fundamental characteristics of plasma turbulence from first principles.

Acknowledgements

This material is based upon work supported by the National Science Foundation Graduate Research Fellowship Program under grant no 1048957, NSF PHY-10033446, NSF CAREER AGS-1054061 and DOE DE-SC0014599. This work used the Extreme Science and Engineering Discovery Environment (XSEDE), which is supported by National Science Foundation grant no. ACI-1053575, through NSF XSEDE Award PHY090084.

REFERENCES

ABEL, I. G., BARNES, M., COWLEY, S. C., DORLAND, W. & SCHEKOCHIHIN, A. A. 2008 Linearized model Fokker–Planck collision operators for gyrokinetic simulations. I. Theory. *Phys. Plasmas* **15** (12), 122509.

BARNES, M., ABEL, I. G., DORLAND, W., ERNST, D. R., HAMMETT, G. W., RICCI, P., ROGERS, B. N., SCHEKOCHIHIN, A. A. & TATSUNO, T. 2009 Linearized model Fokker–Planck collision operators for gyrokinetic simulations. II. Numerical implementation and tests. *Phys. Plasmas* **16** (7), 072107.

BOROVSKY, J. E. & DENTON, M. H. 2011 No evidence for heating of the solar wind at strong current sheets. *Astrophys. J. Lett.* **739**, L61.

DRAKE, D. J., HOWES, G. G., RHUDY, J. D., TERRY, S. K., CARTER, T. A., KLETZING, C. A., SCHROEDER, J. W. R. & SKIFF, F. 2016 Measurements of the nonlinear beat wave produced by the interaction of counterpropagating Alfven waves. *Phys. Plasmas* **23** (2), 022305.

DRAKE, D. J., SCHROEDER, J. W. R., HOWES, G. G., KLETZING, C. A., SKIFF, F., CARTER, T. A. & AUERBACH, D. W. 2013 Alfvén wave collisions, the fundamental building block of plasma turbulence. IV. Laboratory experiment. *Phys. Plasmas* **20** (7), 072901.

FRIEMAN, E. A. & CHEN, L. 1982 Nonlinear gyrokinetic equations for low-frequency electromagnetic waves in general plasma equilibria. *Phys. Fluids* **25**, 502–508.

GALTIER, S., NAZARENKO, S. V., NEWELL, A. C. & POUQUET, A. 2000 A weak turbulence theory for incompressible magnetohydrodynamics. *J. Plasma Phys.* **63**, 447–488.

GOLDREICH, P. & SRIDHAR, S. 1995 Toward a theory of interstellar turbulence II. Strong Alfvénic turbulence. *Astrophys. J.* **438**, 763–775.

HOWES, G. G. 2016 The dynamical generation of current sheets in astrophysical plasma turbulence. *Astrophys. J. Lett.* **827**, L28.

HOWES, G. G. 2017 Ronald C. Davidson award 2016: a prospectus on kinetic heliophysics. *Phys. Plasmas* **24** (5), 055907.

HOWES, G. G. & BOUROUAINE, S. 2017 The development of magnetic field line wander by plasma turbulence. *J. Plasma Phys.* **83** (4), 905830408.

HOWES, G. G., COWLEY, S. C., DORLAND, W., HAMMETT, G. W., QUATAERT, E. & SCHEKOCHIHIN, A. A. 2006 Astrophysical gyrokinetics: basic equations and linear theory. *Astrophys. J.* **651**, 590–614.

HOWES, G. G., DRAKE, D. J., NIELSON, K. D., CARTER, T. A., KLETZING, C. A. & SKIFF, F. 2012 Toward astrophysical turbulence in the laboratory. *Phys. Rev. Lett.* **109** (25), 255001.

HOWES, G. G., KLEIN, K. G. & LI, T. C. 2017 Diagnosing collisionless energy transfer using wave-particle correlations: Vlasov-Poisson plasmas. *J. Plasma Phys.* **83** (1), 705830102.

HOWES, G. G., MCCUBBIN, A. J. & KLEIN, K. G. 2018 Spatial localization of particle energization in current sheets produced by Alfvén wave collisions. *J. Plasma Phys.* **84** (1), 905840105.

HOWES, G. G. & NIELSON, K. D. 2013 Alfvén wave collisions, the fundamental building block of plasma turbulence. I. Asymptotic solution. *Phys. Plasmas* **20** (7), 072302.

HOWES, G. G., NIELSON, K. D., DRAKE, D. J., SCHROEDER, J. W. R., SKIFF, F., KLETZING, C. A. & CARTER, T. A. 2013 Alfvén wave collisions, the fundamental building block of plasma turbulence. III. Theory for experimental design. *Phys. Plasmas* **20** (7), 072304.

IROSHNIKOV, R. S. 1963 The turbulence of a conducting fluid in a strong magnetic field. *Astron. Zh.* **40**, 742; English Translation: *Sov. Astron.* **7**, 566 (1964).

KARIMABADI, H., ROYTERSHTEYN, V., WAN, M., MATTHAEUS, W. H., DAUGHTON, W., WU, P., SHAY, M., LORING, B., BOROVSKY, J., LEONARDIS, E. *et al.* 2013 Coherent structures, intermittent turbulence, and dissipation in high-temperature plasmas. *Phys. Plasmas* **20** (1), 012303.

KLEIN, K. G. & HOWES, G. G. 2016 Measuring collisionless damping in heliospheric plasmas using field-particle correlations. *Astrophys. J. Lett.* **826**, L30.

KLEIN, K. G., HOWES, G. G. & TENBARGE, J. M. 2017 Diagnosing collisionless energy transfer using field-particle correlations: gyrokinetic turbulence. *J. Plasma Phys.* **83** (4), 535830401.

KRAICHNAN, R. H. 1965 Inertial range spectrum of hyromagnetic turbulence. *Phys. Fluids* **8**, 1385–1387.

MATTHAEUS, W. H. & MONTGOMERY, D. 1980 Selective decay hypothesis at high mechanical and magnetic Reynolds numbers. *Ann. N.Y. Acad. Sci.* **357**, 203–222.

MENEGUZZI, M., FRISCH, U. & POUQUET, A. 1981 Helical and nonhelical turbulent dynamos. *Phys. Rev. Lett.* **47**, 1060–1064.

MONTGOMERY, D. & MATTHAEUS, W. H. 1995 Anisotropic modal energy transfer in interstellar turbulence. *Astrophys. J.* **447**, 706.

NG, C. S. & BHATTACHARJEE, A. 1996 Interaction of shear-Alfven wave packets: implication for weak magnetohydrodynamic turbulence in astrophysical plasmas. *Astrophys. J.* **465**, 845.

NIELSON, K. D. 2012 Analysis and gyrokinetic simulation of MHD Alfven wave interactions. PhD thesis, The University of Iowa.

NIELSON, K. D., HOWES, G. G. & DORLAND, W. 2013 Alfvén wave collisions, the fundamental building block of plasma turbulence. II. Numerical solution. *Phys. Plasmas* **20** (7), 072303.

NUMATA, R., HOWES, G. G., TATSUNO, T., BARNES, M. & DORLAND, W. 2010 AstroGK: astrophysical gyrokinetics code. *J. Comput. Phys.* **229**, 9347.

OSMAN, K. T., MATTHAEUS, W. H., GOSLING, J. T., GRECO, A., SERVIDIO, S., HNAT, B., CHAPMAN, S. C. & PHAN, T. D. 2014 Magnetic reconnection and intermittent turbulence in the solar wind. *Phys. Rev. Lett.* **112** (21), 215002.

OSMAN, K. T., MATTHAEUS, W. H., GRECO, A. & SERVIDIO, S. 2011 Evidence for inhomogeneous heating in the solar wind. *Astrophys. J. Lett.* **727**, L11.

OSMAN, K. T., MATTHAEUS, W. H., WAN, M. & RAPPAZZO, A. F. 2012 Intermittency and local heating in the solar wind. *Phys. Rev. Lett.* **108** (26), 261102.

PERRI, S., GOLDSTEIN, M. L., DORELLI, J. C. & SAHRAOUI, F. 2012 Detection of small-scale structures in the dissipation regime of solar-wind turbulence. *Phys. Rev. Lett.* **109** (19), 191101.

SRIDHAR, S. & GOLDREICH, P. 1994 Toward a theory of interstellar turbulence. 1: weak Alfvenic turbulence. *Astrophys. J.* **432**, 612–621.

TENBARGE, J. M. & HOWES, G. G. 2013 Current sheets and collisionless damping in kinetic plasma turbulence. *Astrophys. J. Lett.* **771**, L27.

URITSKY, V. M., POUQUET, A., ROSENBERG, D., MININNI, P. D. & DONOVAN, E. F. 2010 Structures in magnetohydrodynamic turbulence: detection and scaling. *Phys. Rev.* E **82** (5), 056326.

VERNIERO, J. L., HOWES, G. G. & KLEIN, K. G. 2018 Nonlinear energy transfer and current sheet development in localized Alfvén wavepacket collisions in the strong turbulence limit. *J. Plasma Phys.* **84** (1), 905840103.

WAN, M., MATTHAEUS, W. H., KARIMABADI, H., ROYTERSHTEYN, V., SHAY, M., WU, P., DAUGHTON, W., LORING, B. & CHAPMAN, S. C. 2012 Intermittent dissipation at kinetic scales in collisionless plasma turbulence. *Phys. Rev. Lett.* **109** (19), 195001.

WANG, X., TU, C., HE, J., MARSCH, E. & WANG, L. 2013 On intermittent turbulence heating of the solar wind: differences between tangential and rotational discontinuities. *Astrophys. J. Lett.* **772**, L14.

WU, P., PERRI, S., OSMAN, K., WAN, M., MATTHAEUS, W. H., SHAY, M. A., GOLDSTEIN, M. L., KARIMABADI, H. & CHAPMAN, S. 2013 Intermittent heating in solar wind and kinetic simulations. *Astrophys. J. Lett.* **763**, L30.

ZHDANKIN, V., UZDENSKY, D. A., PEREZ, J. C. & BOLDYREV, S. 2013 Statistical analysis of current sheets in three-dimensional magnetohydrodynamic turbulence. *Astrophys. J.* **771**, 124.